Chinese Chemical Letters 35 (2024) 109680

Contents lists available at ScienceDirect

Chinese Chemical Letters

journal homepage: www.elsevier.com/locate/cclet

Gas-generating polymersomes-based amplified photoimmunotherapy for abscopal effect and tumor metastasis inhibition

Chenlu Huang, Xinyu Yang, Qingyu Yu, Linhua Zhang*, Dunwan Zhu*

Tianjin Key Laboratory of Biomedical Materials, Key Laboratory of Biomaterials and Nanotechnology for Cancer Immunotherapy, Institute of Biomedical Engineering, Chinese Academy of Medical Sciences & Peking Union Medical College, *Tianjin 300192*, *China*

ARTICLE INFO

Article history:
Received 16 January 2024
Revised 17 February 2024
Accepted 18 February 2024
Available online 8 March 2024

Keywords:
Polymersomes
Phototherapy
Immunotherapy
TLR 7/8 agonist
Gas-generating

ABSTRACT

Due to the heterogeneity of tumors, single phototherapy cannot completely ablate tumors and inhibit tumor metastasis. To overcome these, we formulated targeted and multifunctional polymersomes ABC@ICG-IMQ-LHRH (AIRL) that encapsulated Toll-like receptor (TLR) 7/8 agonist imiquimod (IMQ) and photosensitizer indocyanine green (ICG) in the hydrophobic layer as well as bubble-generator NH_4HCO_3 in the hydrophilic cavity to inhibit the growth of primary and distant tumors, and prevent tumor metastasis through synergistic photoimmunotherapy. The AIRL polymersomes exhibited uniform and stable size, and high drug encapsulation efficiency, acid/reduction/laser responsiveness, excellent photothermal conversion efficiency, effective reactive oxygen species generation, high tumor accumulation. AIRL could be effectively internalized by dendritic cells (DCs), achieve lysosome escape and enhance DCs maturation. The synergistic photoimmunotherapy *via* AIRL polymersomes remarkably promoted the differentiation and activation of T cells, elevated strong systemic immune response to eradicate primary tumors and inhibit the growth of distant tumors. Simultaneously, the endurable immunological memory prevented tumor metastasis, which provided a promising nanoplatform for the combination therapy of cancer.

Compared with the traditional cancer treatments, phototherapy, including photothermal therapy (PTT) and photodynamic therapy (PDT), has been extensively studied in recent years due to some certain advantages such as spatiotemporal controllability, negligible drug resistance, low cumulative toxicity, and non-invasiveness [1,2]. PTT makes use of photosensitizers to generate hyperthermia from near-infrared (NIR) laser cause tumor cell damage [3,4]. Previous studies have proved that tumor tissues are more sensitive for hyperthermia and easier to cause irreversible damage than normal tissues. And PDT can transduce light energy into reactive oxygen species (ROS), which induces tumor cell apoptosis directly [5]. With outstanding biocompatibility, potential biodegradability, strong NIR absorption and excellent photothermal conversion efficiency, organic photosensitizers are widely researched in the field of PTT and PDT [6,7]. However, the poor water solubility and light stability hamper the clinical application of organic photosensitizers. The nanocarriers [8–10] can effectively encapsulate the organic photosensitizers and improve its stability in the body, thus enhancing the accumulation in tumor cells. Polymer is a common component of nanocarriers, which can form micelles, polymersomes and other nanocarriers through self-assembly method, showing a wide potential in tumor therapy [11,12].

Nanocarrier-mediated PTT/PDT has superior efficacy for primary tumor ablation, but there is low efficacy in inhibiting tumor metastasis and recurrence [9,13,14]. Notably, researches have indicated that PTT/PDT can stimulate weak immune response *via* releasing tumor-associated antigen (TAA) and the introduction of immune adjuvants can amplify the antitumor immunity, which is fundamental for suppression of tumor metastasis and recurrence [15,16]. Imiquimod (IMQ) as Toll-like receptor (TLR) 7/8 agonist has been approved by Food and Drug Administration (FDA), which can induce dendritic cells (DCs) maturation and augment migration ability of DCs *via* myeloid differentiation factor 88 (MyD88)-dependent pathways as well as further promote TAA presentation, thus stimulating the proliferation and differentiation of $CD8^+/CD4^+$ T cells [17–20]. Lysosomal escape can promote the cross-presentation of antigens and thus enhance the activation of cytotoxic T cells (CTLs), which is crucial to trigger powerful immune effect. Studies have shown that the release of gases or ions in the endosomal environment can destroy the lysosomal membrane and promote the release of drugs into the cytoplasm [21–23], showing a positive effect on immune response.

* Corresponding authors.
E-mail addresses: zhanglinhua@bme.pumc.edu.cn (L. Zhang), zhudunwan@bme.pumc.edu.cn (D. Zhu).

https://doi.org/10.1016/j.cclet.2024.109680
1001-8417/

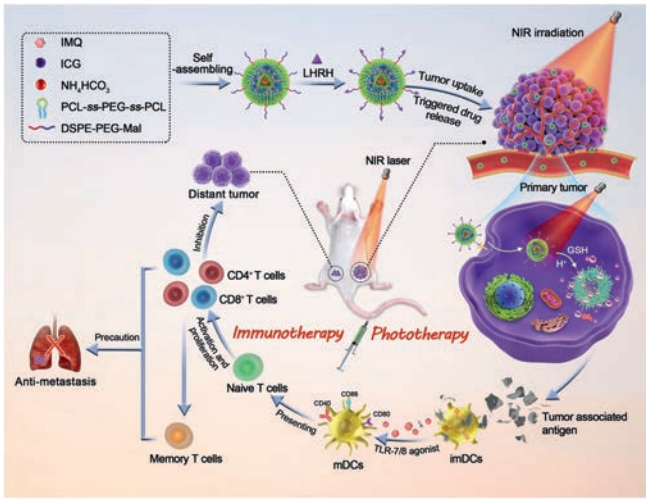

Fig. 1. Schematic illustration of multifunctional polymersomes AIRL for combined phototherapy and immunotherapy against colon tumor.

Herein, we developed an acid/glutathione (GSH)-responsive gas-generating polymersomes to co-deliver photosensitizer indocyanine green (ICG) and TLR 7/8 agonist IMQ for the realization of combined phototherapy and immunotherapy, which can effectively inhibit primary and distant tumor growth and prevent tumor metastasis (Fig. 1). In brief, we constructed polymersomes ABC@ICG-IMQ (AIR) based on poly(ε-caprolactone)-*ss*-poly(ethylene glycol)-*ss*-poly(ε-caprolactone) (PCL-*ss*-PEG-*ss*-PCL) using thin-film hydration and ultrasonic dispersion method. The hydrophobic film layer was loaded with IMQ and ICG, and the hydrophilic inner cavity was encapsulated with the bubble forming agent NH_4HCO_3, which could accelerate drug release under the acidic environment or NIR irradiation. In addition, the surface of the AIR polymersomes was modified with LHRH peptides to enhance the recognition and binding ability on tumor cells [24,25], thus improving the stability and biological distribution of AIRL *in vivo*, further enhancing the therapeutic effect. AIRL-mediated phototherapy plus immunotherapy not only significantly inhibited the growth of primary and distant tumors, but also prevented tumor metastasis by inducing potent immune memory. Therefore, the multifunctional polymersomes AIRL-mediated synergistic photoimmunotherapy may be a promising treatment for cancer.

The multifunctional polymersomes ABC@ICG-IMQ-LHRH (AIRL) were self-assembled from PCL_{7500}-*ss*-PEG_{7500}-*ss*-PCL_{7500}, ICG, IMQ, NH_4HCO_3, and LHRH by the thin-film hydration and sonication method, which ICG and IMQ were encapsulated in the hydrophobic layer while NH_4HCO_3 was loaded in the hydrophilic core. The prepared AIRL was dark green, homogeneous solution with apparent Tyndall effect (Fig. 2A). The particle size of AIRL was between 100 nm and 150 nm and kept stable within a week, which could achieve high accumulation into the tumor site through enhanced permeability and retention (EPR) effect (Fig. 2B) [26,27]. Then, the responsiveness of AIRL was evaluated by detecting the size changes in different conditions. As shown in Fig. 2C, the size of AIRL distributed with a narrow peak in phosphate buffer solution (PBS, pH 7.4) and the peak became broadened in PBS (pH 5.5). Disulfide bonds cleaved under the condition of reduction resulting in polyethylene glycol (PEG) shedding from the nanoparticles, causing a small peak appeared. In addition, the structure of AIRL was further broken under the condition of irradiation and exhibited two broad peaks, demonstrating AIRL with acid/reduction/laser sensitivity. AIRL with high negative charge (-23.37 ± 0.75 mV) could prolong circulating half-lives [28]. The encapsulation efficiencies of ICG and IMQ in AIRL were 88.19% ± 1.90% and 78.51% ± 1.44%, respectively. Fig. 2D showed that the ultraviolet–visible (UV–vis) absorption spectrum of free ICG decreased rapidly within 7 days. While the absorbance of AIRL remained constant, indicating the polymersomes improved the stability of ICG (Fig. 2E). 1,3-Diphenylisobenzofuran (DPBF) was utilized to evaluate the generated ROS level and the absorbance values of DPBF in AIRL and free ICG solutions gradually decreased within 5 min under the irradiation of 808 nm laser (1.5 W/cm^2), demonstrating ICG-encapsulated polymersomes had a good PDT effect (Fig. 2F). AIRL polymersomes exhibited concentration and laser irradiation power-dependent temperature elevation abilities (Fig. S1 in Supporting information). The temperature variation curves of different formulations under 808 nm laser (1.5 W/cm^2) were shown in Fig. 2G. Due to irreversible photobleaching of ICG exposed to laser irradiation, ICG-encapsulated polymersomes exhibited higher temperature elevation than free ICG [29]. The PTT stability of AIRL was evaluated by three laser irradiation on/off cycles (Fig. 2H), during the three cycles, the maximum temperatures of AIRL were 57.0, 53.9, and 44.0 °C, while those of free ICG were 47.6, 36.5, and 36.3 °C, respectively.

The cellular uptake was visualized by confocal laser scanning microscope (CLSM). As shown in Fig. S2 (Supporting information), free ICG exhibited the most inferior red fluorescence intensity compared to polymersomes-treated group. AIRL showed more superior intracellular accumulation than AIR whether with or without laser irradiation, suggesting that LHRH-modified polymersomes had higher CT26 tumor selectivity. The polymersomes with laser irradiation significantly enhanced the uptake of ICG in CT26 cells compared to non-laser groups, probably attributing to that the laser-caused hyperthermia could improve cytomembrane permeability and fluidity, and disrupt polymersomes into smaller pieces, thus increasing the drug accumulation in tumor cells and promoting ICG release from polymersomes [30]. Generation of ROS in CT26 cells was detected using carboxy-H_2DCFDA. Without laser irradiation, fluorescence signal was not observed in all the treatment groups (Fig. S3 in Supporting information). While laser irradiation was carried out, the groups of free ICG, AIR, and AIRL all exhibited enhanced fluorescence signals, indicating cytotoxic ROS was produced. Moreover, due to the active-targeting effect of LHRH, AIRL increased the ROS level in CT26 cells, illustrating that AIRL enhanced the PDT effect.

Biodistribution behavior of polymersomes was investigated in CT26 tumor-bearing mice after intravenous (i.v.) injection. All animal experiments were conducted in accordance with the guidelines for the Animal Ethical and Welfare Committee of the Institute of Radiation Medicine, Chinese Academy of Medical Sciences, with approval number IRM-DWLL-2019167. As shown in Fig. S4 (Supporting information), fluorescence signals of all groups at tumor site progressively strengthened over time and reached a peak at 24 h post-injection. Compared with free ICG and AIR groups, much stronger ICG fluorescence in the tumor was observed in mice i.v. injection with AIRL of 72 h, which indicated that polymersomes effectively prevented ICG from degradation and clearance and further prolonged blood circulation in the body [31]. The results also showed that AIRL achieved excellent accumulation in the tumor site through active targeting effect of LHRH. To further discover the generation of ROS *in vivo*, 2′,7′-dichlorodihydrofluorescein diacetate (DCFH-DA) probe was utilized. As shown in Fig. S5 (Supporting information), AIRL group generated more ROS (green fluorescence) under NIR laser irradiation as a result of higher tumor-targeting efficiency. Due to aggregation and degradation *in vivo* and poor photostability, free ICG was difficult to accumulate in tumor and produced negligible ROS.

DCs as the most potent antigen-presenting cells (APCs) are responsible for initiating and regulating adaptive immunities, which

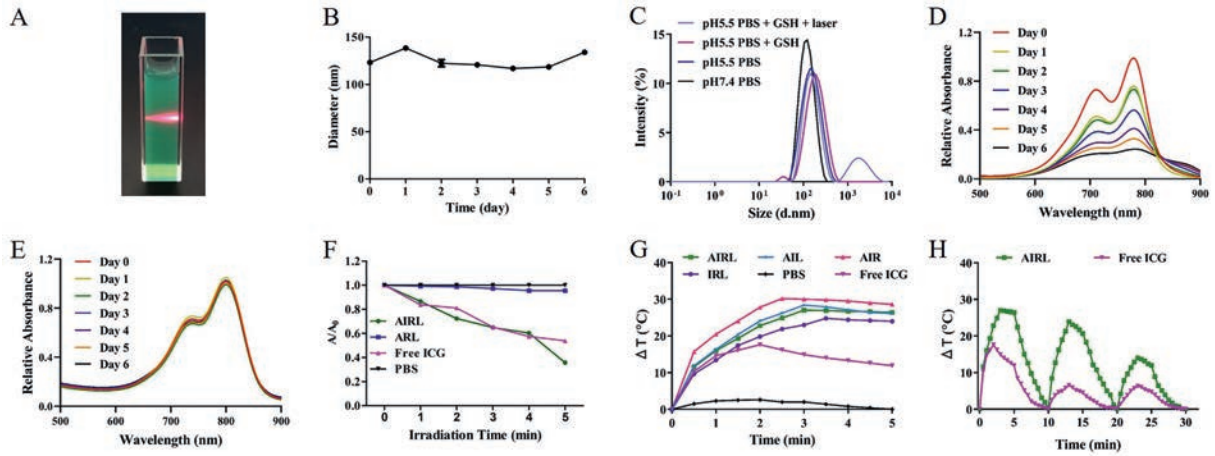

Fig. 2. Preparation and characterization of AIRL. (A) Tyndall effect of AIRL solution. (B) Particle size stability of AIRL in PBS (pH 7.4) over 7 days. (C) Size changes of AIRL in different conditions. UV–vis spectra of (D) free ICG and (E) AIRL over 7 days. (F) Relative absorbance of DPBF in AIRL, ARL, free ICG, and PBS solutions under NIR irradiation over 5 min. (G) Photothermal effect of AIRL, AIL, AIR, IRL, PBS, and free ICG under NIR irradiation (808 nm, 1.5 W/cm^2). (H) Photothermal stability test of AIRL and free ICG under three laser irradiation on/off cycles (808 nm, 1.5 W/cm^2).

could express high levels of antigen bound MHC I and MHC II molecules and costimulatory molecules (CD40, CD80, CD86) on the surface of cells, as well as secret immunostimulatory cytokines with the help of TLR 7/8 agonists [32–34]. We first studied the potential cytotoxicity of polymersomes on DCs *in vitro* by using APC Annexin V Apoptosis Detection Kit with 7-AAD. The result demonstrated that polymersomes and free ICG + IMQ did not affect the survival of bone marrow-derived dendritic cells (BMDCs) (Fig. S6A in Supporting information). Besides, cellular uptake of AIRL was evaluated on DCs. The uptake efficiency of free ICG + IMQ was 24.7%, while this of IRL and AIRL were 27.7% and 39.7%, respectively, which illustrated that gas generation function could promote the uptake of nanocarrier by DCs (Figs. S6B and C in Supporting information). The CLSM images showed the green fluorescence of ICG overlapped with the red fluorescence of lysosome in free ICG + IMQ group, suggesting free ICG + IMQ colocalized with lysosome in DCs (Fig. S6D in Supporting information). The colocalization level of AIRL group was less than that of IRL group, probably due to that NH_4HCO_3 reacted with H^+ in the acidic environment of lysosome and generated CO_2 bubble, leading to lysosome escape.

Next, the effects of AIRL polymersomes toward DCs maturation *in vitro* were analyzed. As shown in Figs. S7 and S8 (Supporting information), compared with free IMQ + ICG, IRL and AIRL polymersomes both upregulated the expression of CD80, CD86, CD40, MHC I and MHC II molecules on the surface of DCs as well as promoted the secretion of tumor necrosis factor (TNF)-α. Necrotic or apoptotic tumor cells after phototherapy treatment can act as TAA to stimulate DCs maturation and further activate tumor-specific immune responses. Therefore, a transwell system was applied to investigate if AIRL-mediated phototherapy could induce the maturation of BMDCs (Fig. S9A in Supporting information). As shown in Figs. S9B–G and S10 (Supporting information), we found that CT26 cells cocultured with AIL polymersomes under laser irradiation could induce DCs maturation slightly. While the CT26 cells cocultured with AIRL and IRL polymersomes under laser irradiation promoted DCs maturation with the help of IMQ [17]. Notably, AIRL significantly stimulated DCs maturation compared with IRL as a result of gas-induced lysosome escape. These results demonstrated that bubble generator- and IMQ-encapsulated polymersomes could significantly promote BMDCs maturation and further trigger antigen-specific immune responses through TAA from necrotic or apoptotic tumor cells post phototherapy.

To explore the mechanism of antitumor immune responses triggered by AIRL polymersomes-based photoimmunotherapy *in vivo*, the splenocytes of mice were collected on the 15th day after first administration (Fig. 3A). CTLs ($CD3^+CD8^+$) kill tumor cells by secreting inflammatory cytokines, while T helper cells (Ths, $CD3^+CD4^+$) can control cellular immunity and activate effector immune cells against tumor [35,36]. Notably, the populations of $CD4^+$ and $CD8^+$ T cells in mice treated with AIRL + laser were 25.9% and 16.2%, which increased over 2-fold compared with those in the mice treated with PBS + laser (Figs. 3B–E). The percentages of Ths and CTLs also increased in mice treated with free ICG + IMQ + laser, IRL + laser and AIR + laser. Additionally, no significant improvement in the populations of $CD4^+$ and $CD8^+$ T cells was found in AIL + laser because of the absence of immune adjuvant IMQ. As an activation molecule of cell surface, CD69 reflects the activation of effector immune cells [37]. As displayed in Figs. 3F and G and Fig. S11 (Supporting information), AIRL + laser treatment appreciably upregulated the percentages of both $CD8^+CD69^+$ and $CD4^+CD69^+$ T cells in the spleen compared with other groups, demonstrating that photoimmunotherapy mediated by AIRL polymersomes with the ability of active-targeting and bubble-generating could stimulate robust tumor-specific immune responses. The populations of both $CD8^+CD69^+$ and $CD4^+CD69^+$ effector T cells greatly increased after the treatment with AIRL + laser compared to AIL + laser treatment, which indicated that immune adjuvant-loaded polymersomes-assisted phototherapy treatment played a crucial role in promoting T cell activation. Moreover, free ICG + IMQ and AIRL groups without laser irradiation treatment hardly activated $CD8^+$ and $CD4^+$ T cells.

The AIRL polymersomes-based treatment schedule was shown in Fig. 4A. Representative thermographic images indicated that the maximum temperature of PBS + laser, free ICG + IMQ + laser, AIL + laser, IRL + laser, AIR + laser, AIRL + laser group at 24 h post-administration was 40.6, 44.5, 56.6, 51.9, 50.4, 56.0 °C, respectively (Fig. 4B). Free ICG + IMQ + laser exhibited moderate temperature elevation, while for ICG-loaded polymersomes + laser groups, the temperature was over 50 °C, which could lead to irreversible damage of tumor cells. Meanwhile, as a result of bubble-generating of NH_4HCO_3 promoted the release of ICG and active-targeting of LHRH enhanced the accumulation of polymersomes in tumor cells, the PTT effect of AIRL was better than IRL and AIR. The maximum temperature of PBS + laser, free ICG + IMQ + laser, AIL + laser, IRL + laser, AIR + laser, AIRL + laser group at 48 h

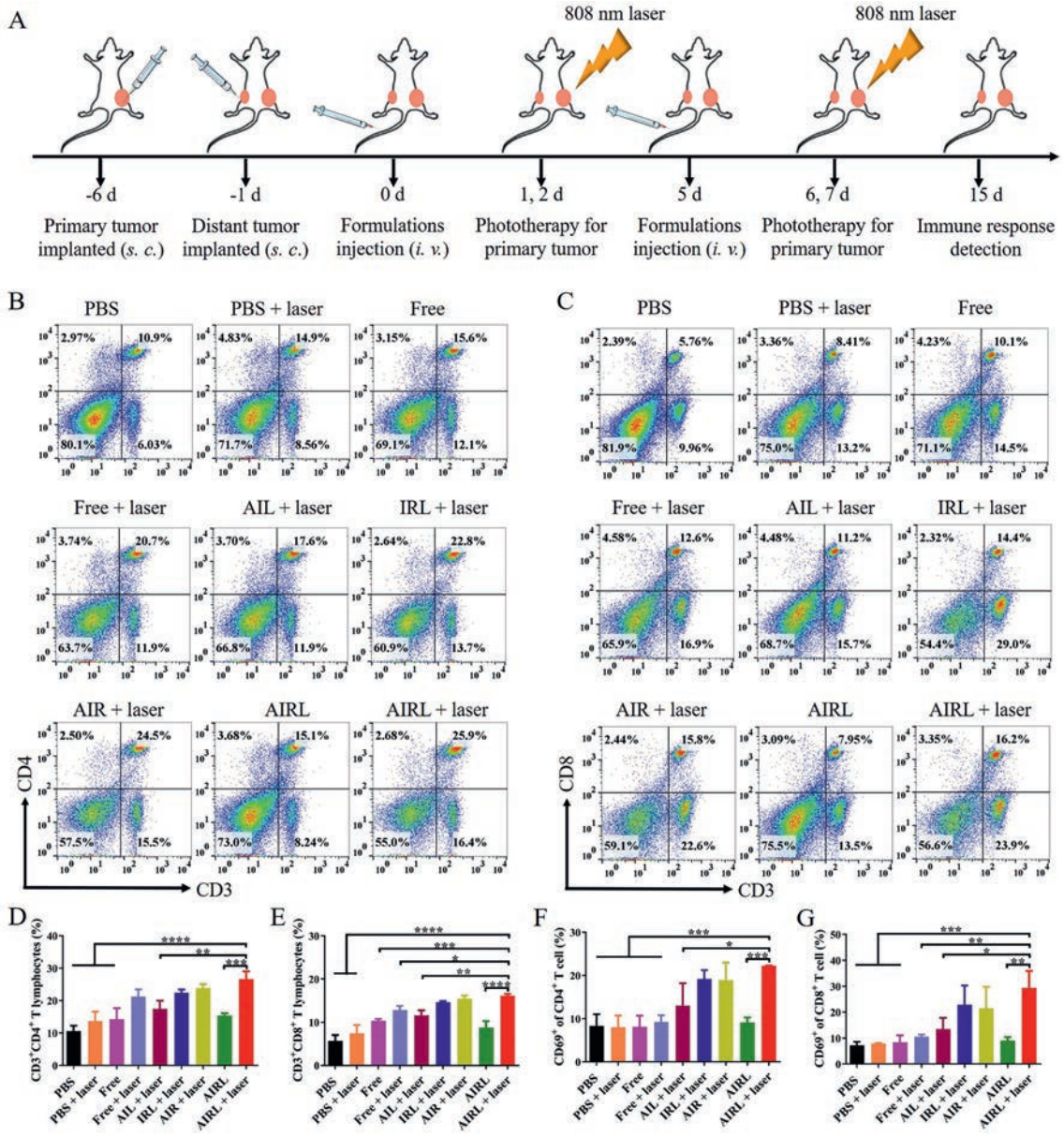

Fig. 3. Analysis of immune effect induced by combination therapy. (A) Schematic illustration of treatment and analysis of immune response. Representative flow cytometry images of (B) $CD3^+CD4^+$ T lymphocytes (Ths) and (C) $CD3^+CD8^+$ T lymphocytes (CTLs) in spleens from the mice treated PBS + laser, free ICG + IMQ + laser ("Free + laser" group), AIL + laser, IRL + laser, AIR + laser, AIRL + laser, PBS, free ICG + IMQ ("Free" group), and AIRL. Analysis of (D) Ths and (E) CTLs in splenocytes ($n = 3$). Proportions of $CD69^+$ cells among (F) $CD3^+CD4^+$and (G) $CD3^+CD8^+$ T lymphocytes in splenocytes ($n = 3$). Data were expressed as mean ± SEM. $^*P < 0.05$, $^{**}P < 0.01$, $^{***}P < 0.001$, $^{****}P < 0.0001$.

post-administration were 38.7, 41.8, 51.4, 46.8, 45.5, 50.4 °C, respectively. The primary and distant tumors grew rapidly after the treatment with PBS or PBS + laser, suggesting that only NIR laser irradiation had no inhibitory effect on CT26 tumors (Fig. 4C and Fig. S12A in Supporting information). Free ICG + IMQ + laser group could slightly delay the growth of primary tumors, while the free ICG + IMQ group showed no obvious effect on the growth of primary tumors. AIRL group exhibited no inhibitory effect on primary and distant tumors, suggesting that AIRL polymersomes without laser irradiation could not exert sufficient antitumor efficacy. In contrast, AIL + laser, IRL + laser, AIR + laser, AIRL + laser groups completely eliminated the primary tumors, exhibited appreciably stronger antitumor efficacy compared with free ICG + IMQ + laser group. Notably, the treatment of AIL + laser, IRL + laser, AIR + laser group showed only a certain delay for the growth of distant tumors, while AIRL + laser group had a better effect for suppressing the growth of distant tumors (Fig. 4D, Fig. S12B in Supporting information). These results indicated that the active targeting of LHRH and the bubble-generating function of NH_4HCO_3 could promote the release of ICG and IMQ in the tumor site and display a remarkable antitumor efficacy for both primary and distant tumors by photoimmunotherapy. During the treatment period, compared with PBS, PBS + laser, free ICG + IMQ, free ICG + IMQ + laser and AIRL groups, the treatment of AIL + laser, IRL + laser and AIR + laser groups remarkably prolonged survival time of mice (Fig. 4E). Notably, the AIRL + laser treatment group displayed the highest survival percentage of mice, with none of the mice dead until day 38. As shown in Fig. 4F, there was no significant weight loss in all groups. And no apparent histomorphology and pathological changes in the major organs of all the groups (Fig. S13 in Supporting information). These results demonstrated that photoimmunotherapy based on AIRL polymersomes with good bio-

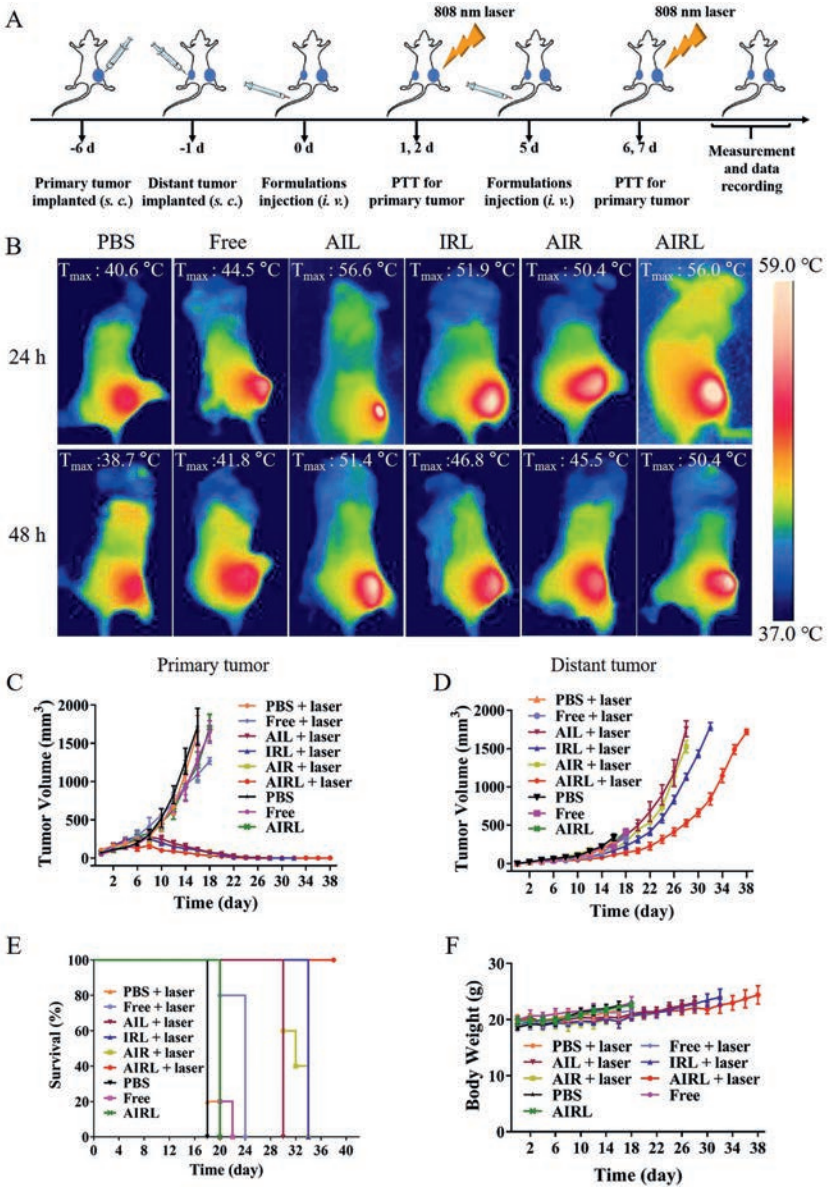

Fig. 4. Antitumor effects of AIRL-mediated phototherapy plus immunotherapy against CT26 tumor. (A) Schematic illustration of establishing CT26 tumor-bearing mice model for antitumor effect. (B) Thermal imaging of tumor-bearing mice treated with PBS, free ICG + IMQ ("Free" group), AIL, IRL, AIR, and AIRL, respectively, and irradiated with NIR laser (808 nm, 1.5 W/cm^2). The volume curves of (C) primary and (D) distant tumor in mice treated with PBS + laser, free ICG + IMQ + laser ("Free + laser" group), AIL + laser, IRL + laser, AIR + laser, AIRL + laser, PBS, free ICG + IMQ ("Free" group), and AIRL ($n = 5$). (E) The percent survival of mice treated with different groups ($n = 5$). (F) Body weight change curves of mice in different groups ($n = 5$). Data were expressed as mean ± SEM.

compatibility could successfully eradicate primary tumor, delay the growth of distant tumor and prolong survival time of CT26 tumor-bearing mice.

In addition to inhibiting tumor growth, the ability of producing long-term immunity is crucial for hampering tumor relapse or metastasis [38]. Memory T cells can protect the organisms from the second attack with the same pathogens and tumor cells as well as play a critical role in preventing recurrence, metastasis of tumor and strengthening immune response [39,40]. Memory T cell is classified into effector-memory T cells (T_{EM}, $CD44^{hi}CD62L^{low}$) and central-memory T cells (T_{CM}, $CD44^{hi}CD62L^{hi}$) [41,42]. To assess the potential of AIRL + laser treatment for inducing immune memory effect, we rechallenged the mice with i.v. injection of CT26 cells on the 21st day post-administration and collected the spleens to analyze memory T cells on the 22nd day (Fig. S14A in Supporting information). The percentages of $CD4^+$ T_{CM} and $CD4^+$ T_{EM} were enhanced in AIRL, AIR, IRL and AIL polymersomes plus laser groups (Figs. S14B, D and E in Supporting information). As shown in Figs. S14C, F and G (Supporting information), similarly, the frequencies of T_{CM} and T_{EM} among $CD8^+$ T cells in AIRL + laser group were strikingly stronger than other groups, indicating that the combination therapy of PTT/PDT and immunotherapy based on AIRL induced the strongest immune memory. Based on the above results, we further investigated the anti-metastatic effect of AIRL-mediated photoimmunotherapy. The lungs of various groups were dissected at the 14th day post i.v. injection of CT26 cells. As shown in Fig. S15 (Supporting information), the photos of lung tissues fixed by Bouin's solution and hematoxylin-eosin (H&E) staining images of lung sections both revealed that no evident tumor nodules were observed in the mice treated with AIRL + laser, AIR + laser and IRL + laser. However, in the other groups, the mice appeared multiple extensive tumor metastasis. These results suggested that pho-

toimmunotherapy based on AIRL polymersomes triggered robust immune memory and significantly inhibited tumor metastasis.

In summary, we developed a targeted and multifunctional polymersomes that co-encapsulated photosensitizer ICG, TLR 7/8 agonist IMQ and bubble-generator NH_4HCO_3 to achieve enhanced photoimmunotherapy against colon tumor. The fabricated polymersomes AIRL with acid/reduction/laser sensitivity could effectively deliver drugs to tumor site and exhibited excellent PTT/PDT effect to kill tumor cells directly under 808 nm laser exposure. Furthermore, AIRL polymersomes dramatically promoted DCs uptake, enhanced lysosomal escape and triggered DCs maturation. The photoimmunotherapy based on AIRL polymersomes significantly increased the activation and differentiation of T cells, and $CD8^+$ CTLs and $CD4^+$ Ths-mediated strong immunity response inhibited primary and distant tumors growth. In addition, the long-term immune memory prevented the mice from tumor metastasis. Therefore, AIRL-mediated photoimmunotherapy showed great potential in suppressing primary tumor growth, metastasis and abscopal effect, which may guide the clinical treatment of cancer.

Declaration of competing interest

The authors declare that they have no competing financial interests or personal relationships that could have appeared to influence the work reported in this paper.

Acknowledgments

This work was financially supported by National Natural Science Foundation of China (Nos. 82172090, 82302390 and 82072059), CAMS Innovation Fund for Medical Sciences (Nos. 2021-I2M-1-058 and 2022-I2M-1-023), China Postdoctoral Science Foundation (No. 2022M720502), Tianjin Municipal Natural Science Foundation (No. 22JCQNJC00070), CAMS Union Young Scholars Support Program (No. 2022051), and Fundamental Research Funds for the Central Universities (No. 2019PT320028).

Supplementary materials

Supplementary material associated with this article can be found, in the online version, at doi:10.1016/j.cclet.2024.109680.

References

[1] Y. Liu, P. Bhattarai, Z. Dai, X. Chen, Chem. Soc. Rev. 48 (2019) 2053–2108.
[2] M. Wang, X. Zhang, B. Liu, et al., Adv. Funct. Mater. 33 (2023) 2300199.
[3] J. Nam, S. Son, L.J. Ochyl, et al., Nat. Commun. 9 (2018) 1074.
[4] R. Vankayala, K.C. Hwang, Adv. Mater. 30 (2018) e1706320.
[5] J. Huang, G. Deng, S. Wang, et al., Adv. Sci. 10 (2023) 2302208.
[6] C. Murugan, V. Sharma, R.K. Murugan, et al., J. Control. Release 299 (2019) 1–20.
[7] J. Qi, Y. Fang, R.T.K. Kwok, et al., ACS Nano 11 (2017) 7177–7188.
[8] L. Huang, Z. Sun, Q. Shen, et al., Chin. Chem. Lett. 33 (2022) 4146–4156.
[9] T. Hu, C. Shen, X. Wang, et al., Chin. Chem. Lett. (2024), doi:10.1016/j.cclet.2024.109562.
[10] T. Liu, H. Zou, J. Mu, et al., Chin. Chem. Lett. 34 (2023) 108135.
[11] W. Li, M. Nakayama, J. Akimoto, T. Okano, Polymer 52 (2011) 3783–3790.
[12] F. Zhang, Y. Hou, M. Zhu, et al., Adv. Sci. 8 (2021) 2102666.
[13] X. Han, R. Wang, J. Xu, et al., Biomaterials 224 (2019) 119490.
[14] Y. Li, J. Cui, C. Li, et al., Chin. Chem. Lett. 34 (2023) 108180.
[15] P. Ji, Y. Gong, M.L. Jin, et al., Sci. Adv. 8 (2022) eabl8247.
[16] Z. Wang, T. You, Q. Su, et al., Adv. Mater. 35 (2023) 2307139.
[17] N.I. Ho, L.G.M. Huis In 't Veld, T.K. Raaijmakers, G.J. Adema, Front. Immunol. 9 (2018) 2874.
[18] M.C. Takenaka, F.J. Quintana, Semin. Immunopathol. 39 (2017) 113–120.
[19] I.Le Mercier, D. Poujol, A. Sanlaville, et al., Cancer Res. 73 (2013) 4629–4640.
[20] A.K. Gupta, A.M. Cherman, S.K. Tyring, J. Cutan. Med. Surg. 8 (2004) 338–352.
[21] M. Tang, B. Chen, H. Xia, et al., Nat. Commun. 14 (2023) 5888.
[22] X. Tang, J. Zhang, D. Sui, et al., J. Control. Release 364 (2023) 529–545.
[23] S. Guo, B. Liu, M. Zhang, et al., Chin. Chem. Lett. 32 (2021) 102–106.
[24] S. Ji, L. Huang, S. Chang, et al., Biomaterials 301 (2023) 122269.
[25] Y. Qin, Q. Guo, S. Wu, et al., Chin. Chem. Lett. 31 (2020) 3121–3126.
[26] L. Wang, Z. Mao, J. Wu, et al., Nano Today 49 (2023) 101782.
[27] Y. Xu, J. Xiong, X. Sun, H. Gao, Acta Pharm. Sin. B 12 (2022) 4327–4347.
[28] E. Blanco, H. Shen, M. Ferrari, Nat. Biotechnol. 33 (2015) 941–951.
[29] W.H. Jian, T.W. Yu, C.J. Chen, et al., Langmuir 31 (2015) 6202–6210.
[30] X. Xue, T. Fang, L. Yin, et al., Drug Deliv. 25 (2018) 1826–1839.
[31] C. Egloff-Juras, L. Bezdetnaya, G. Dolivet, H.P. Lassalle, Int. J. Nanomedicine 14 (2019) 7823–7838.
[32] Q. Zhou, Y. Zhang, J. Du, et al., ACS Nano 10 (2016) 2678–2692.
[33] C. Qian, X. Cao, Semin. Immunol. 35 (2018) 3–11.
[34] R. Huang, P. Zhou, B. Chen, et al., ACS Nano 17 (2023) 21455–21469.
[35] F. Chen, Y. Wang, J. Gao, et al., Biomaterials 270 (2021) 120709.
[36] J.M. Silva, M. Videira, R. Gaspar, et al., J. Control. Release 168 (2013) 179–199.
[37] D.V. Krysko, A.D. Garg, A. Kaczmarek, et al., Nat. Rev. Cancer 12 (2012) 860–875.
[38] J. Yang, C. Zhang, X. Chen, et al., Biomaterials 302 (2023) 122303.
[39] R. De Coen, N. Vanparijs, M.D. Risseeuw, et al., Biomacromolecules 17 (2016) 2479–2488.
[40] W. Shi, W. Feng, S. Li, et al., ACS Nano 17 (2023) 14475–14493.
[41] J. Kaiser, Science 356 (2017) 122.
[42] T. He, M. Hu, S. Zhu, et al., Acta Pharm. Sin. B 13 (2023) 804–818.